atmosphere

Article

Climate Patterns and Their Influence in the Cordillera Blanca, Peru, Deduced from Spectral Analysis Techniques

Adrián Fernández-Sánchez [1,2,*], José Úbeda [1,2], Luis Miguel Tanarro [1], Nuria Naranjo-Fernández [3], José Antonio Álvarez-Aldegunde [4] and Joshua Iparraguirre [5]

1 Departamento de Geografía, Universidad Complutense de Madrid, 28040 Madrid, Spain
2 Guías de Espeleología y Montaña, Casilla del Mortero, s/n, 28189 Madrid, Spain
3 Centro de Hidrogeología, Universidad de Málaga, Ada Byron Investigation Building, Module B, 1st Floor, St. Arquitecto Francisco Peñalosa, 18, 29590 Málaga, Spain
4 Civil Engineering Department, Universidad de Cartagena, St. San Agustín, Cra. 6, Nª 36-100, Cartagena De Indias 130001, Colombia
5 Instituto Geológico, Minero y Metalúrgico, Avenida Canadá, 1470, San Borja, Lima 41, Peru
* Correspondence: adrferna@ucm.es; Tel.: +971-585094518

Abstract: Climate patterns are natural processes that drive climate variability in the short, medium, and long term. Characterizing the patterns behind climate variability is essential to understand the functioning of the regional atmospheric system. Since investigations typically reveal only the link and extent of the influence of climate patterns in specific regions, the magnitude of that influence in meteorological records usually remains unclear. The central Peruvian Andes are affected by most of the common climate patterns of tropical areas, such as Intertropical Convergence Zone (ITCZ), Sea Surface Temperature (SST), solar irradiance, Madden Julian Oscillation (MJO), Pacific Decadal Oscillation (PDO), and El Niño Southern Oscillation (ENSO). They are also affected by regional processes that are exclusive from South America, such as the South American Low-Level Jet (SALLJ), South American Monsoon System (SAMS), Bolivian High (BH), and Humboldt Current. The aim of this research is to study the climate variability of precipitation, maximum and minimum temperature records over Cordillera Blanca (Peru), and its relationship with the intensity and periodicity of the common climate patterns that affect this region. To achieve this aim, a spectral analysis based on Lomb's Periodogram was performed over meteorological records (1986–2019) and over different climate pattern indexes. Results show a coincidence in periodicity between MJO and SALLJ, with monthly cycles for precipitation and temperature (27-day, 56-day, and 90-day cycles). Moreover, the most intense periodicities, such as annual (365 days) and biannual (182 and 122 days) cycles in meteorological variables, possibly would be led by ITCZ and ENSO together, as well as a combination of the Humboldt Current and SALLJ. Additionally, interannual periodicities (3-year, 4.5-year, 5.6–7-year and 11-year cycles) would have coincidence with the ENSO–solar combination, while the longest cycles (16 years) could match PDO variability.

Keywords: Peru climate; climate patterns; spectral analysis; Lomb's periodogram; climatology; ENSO; ITCZ; SALLJ

Citation: Fernández-Sánchez, A.; Úbeda, J.; Tanarro, L.M.; Naranjo-Fernández, N.; Álvarez-Aldegunde, J.A.; Iparraguirre, J. Climate Patterns and Their Influence in the Cordillera Blanca, Peru, Deduced from Spectral Analysis Techniques. *Atmosphere* **2022**, *13*, 2107. https://doi.org/10.3390/atmos13122107

Academic Editor: Anthony R. Lupo

Received: 15 November 2022
Accepted: 14 December 2022
Published: 16 December 2022

1. Introduction

Climate patterns such as marine currents, monsoons, atmospheric configurations, or low level winds lead climate variability at a short and mean term. It also can be considered as the climate patterns of solar irradiation [1], the El Niño Southern Oscillation (ENSO) phenomena, or the latitude southward shift of the Intertropical Convergence Zone (ITCZ) [2].

Analysis of the dynamics of climate patterns was found to be of great utility of feeding climate models [3,4], remembering that variations on a global scale are also influenced by regional processes. Characterization of the regional pattern periodicity can help models to

better predict future changes, as relationships between those patterns and different weather configurations need to be clarified. Other studies related the regional climate patterns with current glacier mass balance [5,6] and palaeoclimate weather configuration [7].

Nowadays, the South America climate is influenced by typical natural processes of tropical areas due to its geographical position, such as the latitudinal displacement of the ITCZ, Pacific Decadal Oscillation (PDO), or the Madden Julian Oscillation (MJO). Additionally, South America is affected by specific regional patterns, such as the El Niño–Southern Oscillation (ENSO), the South Atlantic Convergence Zone (SACZ), the South American Monsoon System (SAMS), or the Humboldt Current [8,9]. Sea Surface Temperatures (SST) would also lead most of these climate drivers as a primary force [10,11]. The Andean range modifies the low-level jets (resulting in the South American Low-Level Jet; SALLJ) or the precipitation over the Andean–Amazon feature that creates the Bolivian High (BH). The Peruvian Central Andes, and hence Cordillera Blanca (the study area), are affected by the previously exposed tropical climate patterns, and its own geomorphological characteristics could also modify the influence of those climate drivers.

In the current global climate change context [12], the region's aim of study in this research (Cordillera Blanca), would situate in a temperature rising of +2.8 °C for the RCP 2.6 and +6 °C for RCP 8.5, both scenarios in the year 2100 [12,13]. In a similar way, precipitation could suffer a 15% or even 20% rise, according to both scenarios previously mentioned [13,14], by the end of the century.

Therefore, it is needed to characterize the climate patterns dynamics in order to detect changes in their evolution, and watching the climate change influence on the patterns that drive these natural processes. Most of the research that deals with this fact reveals the extent and relationship between climate drivers and their influence on the region [15–17] or the atmospheric mechanisms that depend on the pattern [18]. Nevertheless, the magnitude and periodicity of the influence of climate patterns in regional meteorological data series usually remain unclear.

Spectral analysis techniques [19] represent an optimal statistical approach for decomposing and identifying periodicities subjacent in data series. Those techniques were widely applied in the Earth sciences field and overall in solar periodicity related research [20–22], but also over air quality data series [23,24], both revealing important controls on climate. In regional studies, spectral analysis was also applied to climate records in order to diagnose the ENSO patterns [25] and to identify the regional structure of precipitation that matches seasonal patterns [26]. Long and complete data series are enough for being subjected to spectral analysis, returning periodicities above a minimum statistical significance level. Therefore, meteorological records or climate indexes (or any other record with variability and a big amount of data) have a great potential for being analyzed.

However, plenty of spectral analysis made of meteorological records from South America does not exist, being mainly palaeoclimatic analysis of sediment cores [27] and ice cores [28,29]. These analyses of periodicities of palaeoclimate proxies are able to determine the regional climate variability, correlating the ciclicities found on proxy data series with the known behavior of climate patterns. Spectral techniques were also applied in the climate study itself, used to characterize the precipitation in the Bolivian Altiplano [30] or to analyze the climatic relationship between places at a long distance, such as Kenya–Ecuador–Hungary [31].

The here proposed data analysis can allow us to characterize the periodicities of the different regional climate pattern magnitudes and relate them to existing periodicities of the same area. Through spectral analysis, the common cycles that rely on different meteorological records can be decomposed and also matched to periodicities of climate patterns. Correlating the meteorological records with the climate patterns can shed light on the regional climatic controls, as some of the influences on climate variability remain unknown. It is not properly understood yet if long distance climate patterns are able to influence in far areas through teleconnections (such as MJO or PDO to some areas of South America), and hence, spectral analysis is able to answer these questions [31].

The aim of this work is to correlate the periodicity of the main climate patterns that affect the Cordillera Blanca of Peru (and middle western South America) with the ciclicities registered over meteorological data series (precipitation, maximum and minimum temperatures) of that mountain range between 1986 and 2019. Common periodicities estimated for climate patterns and meteorological records allowed us to identify the regional climatic controls. Obtained results can be added to the current knowledge on South America's meteorological variability as they clarify the extent of the influence of some climatic teleconnections. The characterization of regional climate variability and teleconnections influence is of particular importance due to the climatic context of Cordillera Blanca that, as a tropical area, is very vulnerable to today's climate change [32,33].

2. Study Area

The present work is based on meteorological data series recorded over Cordillera Blanca (Peruvian Andes) and its surrounding area (Figure 1). Cordillera Blanca is a mountain range located in the Central Andes that extends with a latitude of 8°30′ to 10°10′ S and longitude 77°00′ to 78°00′ W, with a Northwestern–Southeastern direction. The range is located in the Ancash department and is one of the highest Peruvian areas, with an average elevation of 4112 m above sea level. Maximum elevation is located in the summit of Nevado Huascaran (6757 m.a.s.l.) [34], while the minimum is found at 978 m.a.s.l. in the Santa River floodplains, northeast of Cordillera Blanca. There also exist 30 summits with a higher elevation than 6000 m [35].

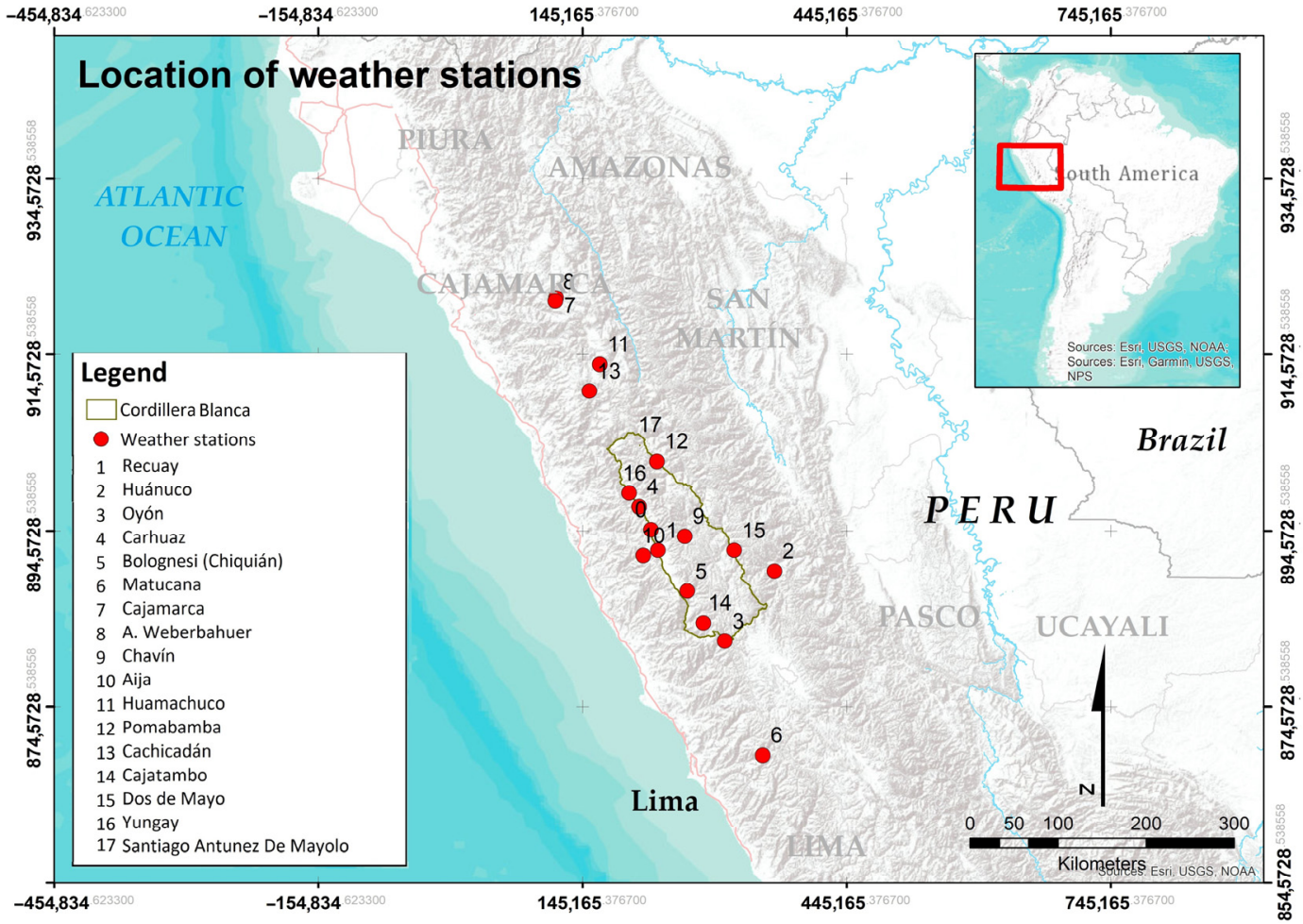

Figure 1. Location of the weather stations of Cordillera Blanca and surrounding areas.

Cordillera Blanca is climatologically influenced by its tropical position and its elevation. In this mountain range, the climate changes according to the rise in altitude, finding semi-arid characteristics in the foothills of the western slopes. In the foothills of Cordillera Blanca, the accumulated average annual precipitation would range between 500 and 1000 mm, while in the summits there would be a fundamentally solid precipitation that would amount to an annual average of 1000 mm [36]. The average annual temperature on the slopes would range between 0 and 6 °C, while on summits would be below 0 °C.

Climate allowed Cordillera Blanca to become the largest area covered by today's tropical glaciers on the planet Earth [37]. The retreatment of those glaciers since the last glacial maximum [38] created over 830 natural lakes with an area of 57.6 Km^2 that feed rivers and channels that are the main freshwater source for more than 1 million people in the department of Ancash [39]. The climate allows a series of changing ecosystems by altitude, such as the so-called "Puna" and "Jalca", located above 3300 m; the "Paramos", located between 3800 to 4500 m.a.s.l.; and cryoturbed soils above 4500 m, composed of unique vegetation [40]. Characterization of climate variability is needed because of the influence that different dynamics could have on water resources and ecosystems, moreover in a changing climate.

3. Materials and Methods

3.1. Materials

For the spectral analysis, up to 17 meteorological stations were chosen (Table 1) covering the Cordillera Blanca area, which contained records of precipitation and maximum and minimum temperatures. The meteorological data were provided by the peruvian meteorological and hydrology service (SENAMHI) and the Agroancash organization. The study period is from 1 January 1986 to 31 December 2019, covering a time series of 34 years, and the raw data provided had a daily time step.

Table 1. Weather stations used in the present study.

Weather Stations	Chosen Period	Variable	Altitude (m.a.s.l)
Aija	1999–2019	P., Max. T, Min.T.	3478
Cachicadan	1986–2019	P., Max. T, Min.T.	2885
Cajamarca	1986–2019	P., Max. T, Min.T.	2686
Cajatambo	1990–2019	P., Max. T, Min.T.	3405
Casapalca	1987–2019	Precipitation	4924
Carhuaz	1986–2016	P., Max. T, Min.T.	2644
Chavín	2000–2019	P., Max. T, Min.T.	3132
Chiquián	1986–2019	P., Max. T, Min.T.	3412
Dos de Mayo	2000–2019	P., Max. T, Min.T.	3474
Huamachuco	1986–2019	P., Max. T, Min.T.	3178
Huánuco	1986–2019	P., Max. T, Min.T.	1918
Matucana	1986–2019	P., Max. T, Min.T.	2417
Oyón	1986–2019	P., Max. T, Min.T.	3663
Pomabamba	1989–2019	P., Max. T, Min.T.	2975
A. Weberbahuer	1986–2019	P., Max. T, Min.T.	2666
Huaraz	1998–2019	P., Max. T, Min.T.	3071
Recuay	1986–2019	P., Max. T, Min.T.	3417

Precipitation (P), Maximum Temperature (Max. T), and Minimum Temperature (Min. T).

At the same time, information was obtained on indicators of the various climatic patterns that most frequently affect the Cordillera Blanca. These data, recorded at daily, monthly, and annual scales, were also subjected to spectral analysis. The indices here consulted (Table 2) were obtained fundamentally from the National Oceanic and Atmospheric Administration of the USA (NOAA), as well as from other published works. Chosen periods for analysis were from 1986 to the most recent date.

Table 2. Indexes and description of the main climate pattern indexes used in the study comparison. Region of the data and source are also shown.

Index	Region	Period
ONI Index (ENSO) [41]	Equatorial Pacific	1950–2021
SST Index [42]	El Niño 1 + 2	1982–2021
Humboldt Current [43]	7–9° S latitude	1997–2017
ITCZ displacement [44]	90–60° W longitude	1979–2005
Outgoing Longwave Radiation [45]	Peruvian Andes	1999–2014
Bolivian High [46]	Bolivia	1979–2014
SALLJ [47]	Eastern Andes	1979–2018
Chocó LLJ [48]	Colombia North	1978–2010
Caribbean LLJ [44]	Caribbean Sea	1979–2010
MJO Index [49]	40° W longitude	1979–2021

The solar activity, the PDO, and the SAMS, were not subjected to spectral analysis due to the large number of recent studies that determined their periodicity.

Both weather and climatic index variables had longer data series available than the chosen period. In the case of Huánuco, Oyón, Augusto Waberbahuer, and Recuay, data started between 1933 and 1964, while the chosen period was 1986–2019. Beginning in 1986 for the climatic analysis allowed more accuracy due to large inconsistencies in the records (non homogenized values, incomplete data, etc.). Nearly all climate index data series started previous to 1986, but in order to select a homogene period with weather records, the 1986–2019 period was chosen for analysis.

3.2. Data Series Preprocessing

The meteorological data series (precipitation and maximum and minimum temperature) were preprocessed based on standardization techniques. These techniques included performing data homogenization and adjustments, the removal of statistically insignificant data, interpolation of data, and statistical imputation of missing and deleted data. It was not necessary that NOAA and other indexes were subjected to homogenization processes, but in the case of Bolivian High and SALLJ, interpolation processes were needed.

The homogenization of the data was carried out only in the stations of Cachicadán (for the variable of precipitation), Casapalca (precipitation), Huánuco (precipitation), Santiago Antúnez de Mayolo (precipitation and minimum temperature), and Augusto Weberbahuer (precipitation and minimum temperature). To carry out the homogenization, the methodology proposed by Martinez et al. [50], was applied to the Huánuco, Oyón, and Chavín stations as a reference based on proximity.

Some meteorological records had missing data, which were completed using statistical imputation techniques proposed by Paulhus and Kohler [51,52]. These techniques were implemented with the Rstudio software [53] from our own code generated for this study.

The formula used in the imputation code is expressed in Equations (1)–(3), and a nearby station with complete data is necessary, which would serve as a reference for temperature variations in the area.

$$Imputed\ T.value = (Coef.a + Coef.b) * Complete\ Station\ Value. \quad (1)$$

where the coefficients a and b are calculated with equations that depend on mean values as follows in Equations (2) and (3).

$$Coef.a = \frac{\widetilde{x}_{incomp} - \sigma_{xy}}{\sigma^2 \cdot \widetilde{x}_{comp}}. \quad (2)$$

$$Coef.b = \frac{\sigma_{xy}}{\widetilde{x}_{comp}} \quad (3)$$

The coefficient "*a*" is the dividing expression between the difference of the mean of the incomplete data series station with the covariance of both stations; while the coefficient "*b*" is the division of the covariance of both stations by the mean of the selected station.

For precipitation, gap filling was also used for the imputation of statistical equations [50]. In this case, two surrounding meteorological stations with complete data were needed, and monthly means of the completed stations were calculated for being integrated in the equation as follows (Equation (4)):

$$Imputed\ P.\ Value = (\left(\frac{1}{3-1}\right) \times \left(\frac{\alpha 1}{\widetilde{x}_{comp1}}\right) + \left(\frac{\alpha 2}{\widetilde{x}_{comp2}}\right). \quad (4)$$

where $\alpha 1$ is the diary value of the reference station number 1, which is one of the stations with completed data, and $\widetilde{x}_{comp1}$ is the monthly mean of that completed station number 1. Again, $\alpha 2$ is the diary value of the completed station number 2, and $\widetilde{x}_{comp2}$ is the monthly mean of that completed station. Both developed codes (supplementary material) were created with Mean Squared Error (MSE) data, which are based on Gauss' proposal of evaluation [54].

The meteorological and climate pattern series were subjected to linear and polynomial adjustments to eliminate trends (detrending) in the short and medium-long term. Meanwhile, the precipitation variable was subjected to an interpolation process. In the case of precipitation, it was necessary to transform the 0 values (equivalent to days without rain) into interpolated values that laid between the actual rain measures [55,56]. This same technique was performed for Bolivian High and SALLJ indexes, as they had 0 values to represent the non-occurrence of BH and SALLJ situations.

3.3. Spectral Analysis

Spectral analysis allows data series to be broken down into cycles that may be superimposed on temporal variability, and they would be difficult to recognize with the naked eye.

The three meteorological variables treated in this study, as well as the climate patterns, were evaluated with the spectral analysis technique using the PAST software [57]. This program uses the Lomb–Scargle periodogram algorithm, which allows for obtaining spectral diagrams with respect to non-equidistant time [19,50].

The results show different maxima and minima peaks related to a periodicity defined according to the spectral power of each period. The analysis also showed a minimum significance or spectral power for each period of the data series, below which the indicated periods do not occur enough times to be decisive. Periodicities were discarded if they did not exceed the given significance. The formula on which the Lomb periodogram is based is shown in Equations (5) and (6).

$$I(\omega_j) = \frac{1}{2s^2}\left\{\frac{\left[\sum_{i=1}^{N}(z(t_i)-m_z)cos\left[\omega_j(t_i-\tau)\right]\right]^2}{\sum_{i=1}^{N}cos^2\left[\omega_j(t_i-\tau)\right]} + \frac{\left[\sum_{i=1}^{N}(z(t_i)-m_z)sin\left[\omega_j(t_i-\tau)\right]\right]^2}{\sum_{i=1}^{N}sin^2\left[\omega_j(t_i-\tau)\right]}\right\}. \quad (5)$$

The τ parameter needs to be resolved in order to make the estimators on the Equation (5) independent from time. That variable is expressed as follows:

$$tan\left[2\omega_j\tau\right] = \frac{\sum_{i=1}^{N}sin\left[2\omega_j t_i\right]}{\sum_{i=1}^{N}cos\left[2\omega_j t_i\right]}. \quad (6)$$

Values m and s^2, are average estimators, the typical deviation is $\{z(t1), z(t2), ..., z(tN)\}$, and wj is the angular frequency in radians for each periodicity. Additionally, $f_j = w_j/(2)$ is the frequency in cycles for each sample interval. The τ parameter makes the estimator of the Equation (6), $I(w_j)$, independent from time. This estimator $I(w_j)$, is Lomb–Scargle's periodogram for the frequency of w_j.

The results of the spectral analysis were expressed, in turn, in maps where a graph is collected with a result for each weather station and a map for each variable.

4. Results

4.1. Analysis of the Spectral Periodicity

This section contains the results of the spectral analysis of the three meteorological variables analyzed. Figure 2. shows a graph of the spectral results with the time periods and the "Power" of each variable for each station, where only those periods higher than the minimum significance (power value between 10 and 12) are represented, depending on each analysis. To facilitate the representation and given the low presence of spectral periods, the results with a period greater than 1000 days are not shown.

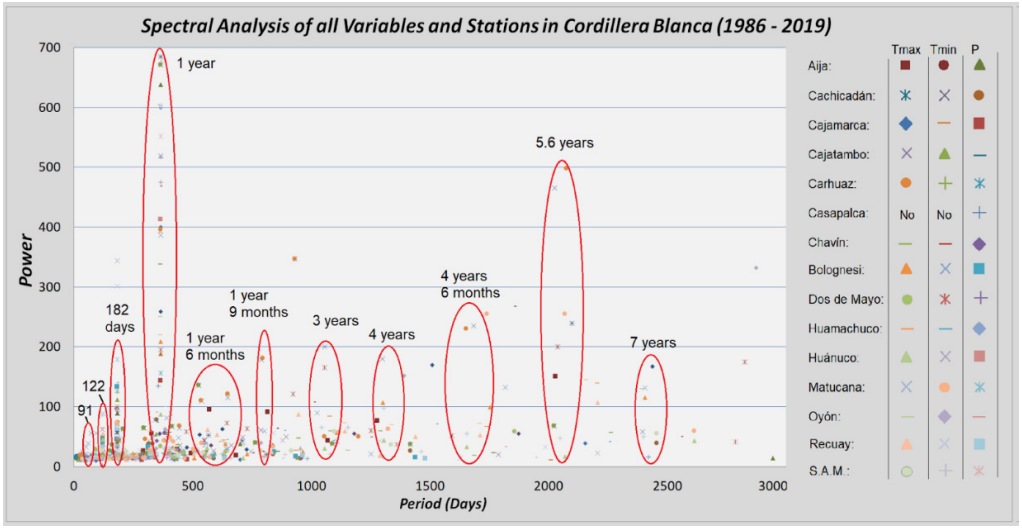

Figure 2. Results for the spectral analysis of each variable and each weather station.

All spectral periods found with sufficient significance are included in the supplementary material. This table shows the periods for all the meteorological stations and the three analysis variables. Tables 3 and 4. are a summary (expanded in the supplementary material), where the spectral periods that coincide in various time ranges are indicated.

Table 3. Identified periodicities for each meteorological variable in an intraseason, interseason, and annual scales.

Variable	Intraseasonal	Intraseasonal	Intraseasonal	Interseasonal	Interseasonal	Annual
Maximum T.	27–30 days	46–52 days	90 days	122 days	182 days	365 days
Minimum T.	27–30 days	46–52 days	90 days	122 days	182 days	365 days
Precipitation	No period	46–52 days	90 days	122 days	182 days	365 days

Table 4. Identified periodicities for each meteorological variable in interannual and interdecadal scales.

Variable	Interannual	Interannual	Interannual	Interannual	Interannual	Interannual	Interdec.	Interdec.
Maximum T.	1 yr 3 m.	1 yr 6 m.	1 yr 9 m.	3 yr	4 yr 6 m	5.6–7 yr	11–12 yr	14–18 yr
Minimum T.	1 yr 3 m.	1 yr 6 m.	1 yr 9 m.	3 yr	4 yr 6 m	5.6–7 yr	11–12 yr	No period
Precipitation	No period	1 yr 3 m.	1 yr 9 m.	No period	No period	5.6–7 yr	11–12 yr	14–18 yr

"T" means temperature, "m" means months, "yr" means year, and "interdec" means interdecadal.

In Figure 2, up to 15 general groups of spectral periods are observed (3 main periods and 12 secondary). The records show very clear spectral signatures in the periods of 122, 182, and 365 days. In the 122-day period, all the stations would present spectral maxima in some of their variables with the exception of the Pomabamba station. The period of

365 days would be observed in all the variables of all the stations, with the exception of the maximum temperature in the Matucana station.

Secondary periods were much more distributed in all the data series and were not coincidental for all the variables and seasons. The following several secondary periods were observed:

- 27 to 30 days (3 months).
- 46 to 52 days (almost a month and a half).
- 90 days (3 months).
- 479 days (1 years and 3 months).
- Between 548 and 560 days (1 year and 6 months).
- 635 days (1 year and 9 months).
- 1095 days (3 years).
- 1460 days (4 years).
- 1650 days (4.5 years).
- Between 2000 and 2555 days (5.6 to 7 years).
- Between 4015 and 4380 days (11 to 12 years).
- Between 5110 and 6570 days (14 to 18 years).

4.2. Spectral Analysis of Main Climatic Patterns

Several climate patterns that most frequently affect the Cordillera Blanca were analyzed with spectral techniques in order to be used in comparison with the meteorological variables.

The spectral analysis of the ONI index, an indicator of ENSO phenomena (Figure 3), yielded five identifiable maximums above the significance P0.01 level. These maximums were 12 months (1 year), 17–20 months (1 year and 5 months to 1 year and 8 months), 39 months (3.25 years), 57–77 months (4.7 to 5.5 years), and 141 months (11.75 years).

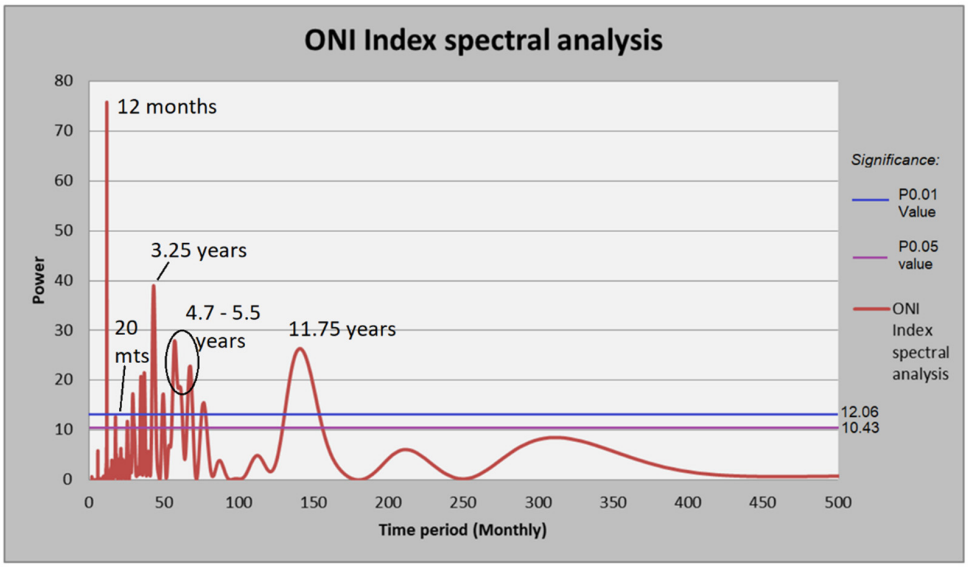

Figure 3. Spectral analysis of the ONI index for the period 1950–2019 on a monthly scale. The red line represents the variability of the spectral power, while the blue line represents the minimum value of significance P0.01 (12.06), and the purple line the minimum value of P0.05 (10.43).

In the matter of the SST (Figure 4), a single cycle of great power is observed, referring to 12 months (1 year). There would be a second cycle of 44 months (4 years), but it would not reach any of the minimum significances, not even the P0.05 significance level.

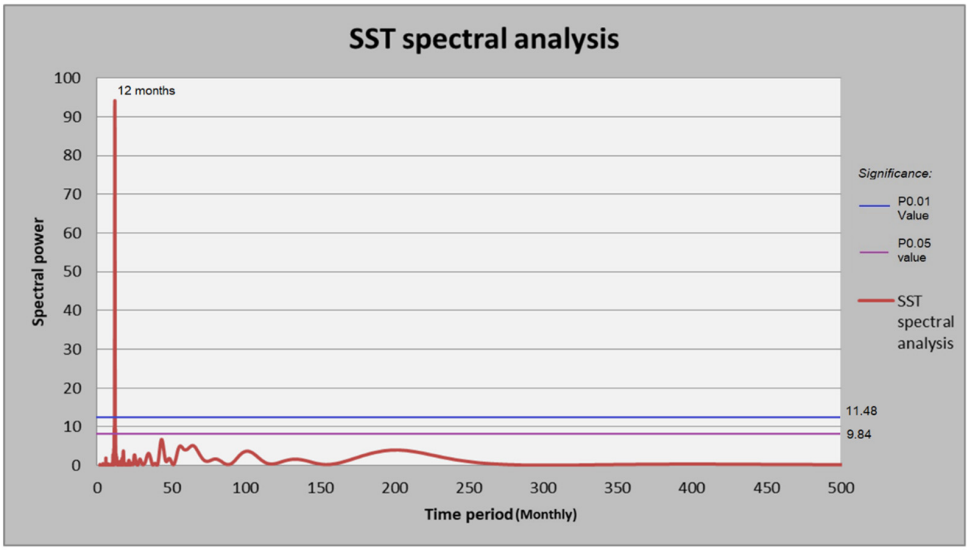

Figure 4. Spectral analysis of the sea surface temperature for the period 1982–2019 on a monthly scale. The red line represents the variability of the spectral power, while the blue line represents the minimum value of significance P0.01 (11.48) and the purple line represents the minimum value of P0.05 (9.84).

In the spectral analysis of the intensity of the Humboldt Current (Figure 5), up to six cycles would be found, in which one of them would be a double cycle, leaving five periodicities. The cycle with the highest power would be the period of 1.18 years (1 year and 1 month), followed by a cycle of 0.86 years (10 months), 0.48 years (6 months), and 0.24 years (4 months). The rest of the long-term periodicities would be 26 months (2.16 years) and 54 months (4.5 years).

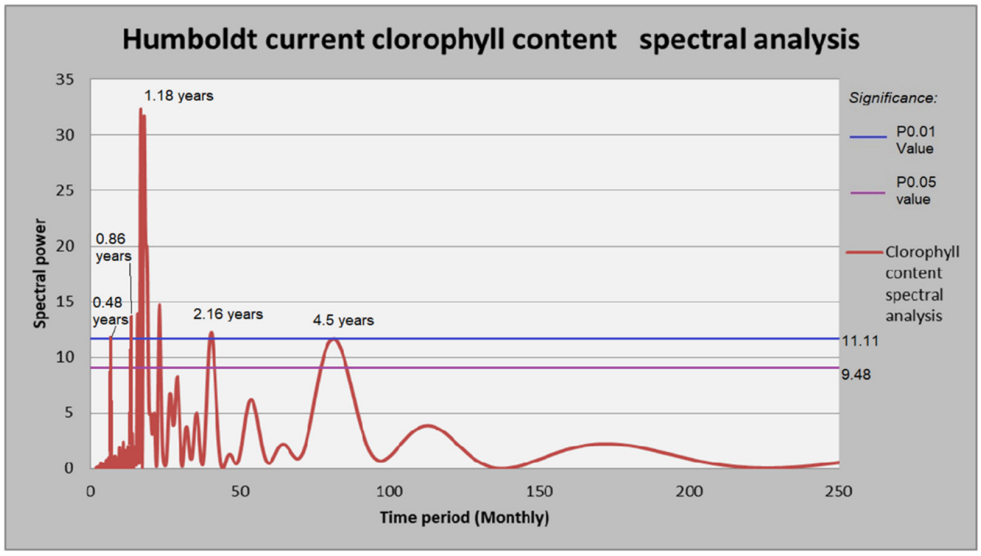

Figure 5. Spectral analysis of the chlorophyll content of the Humboldt Current (intensity) for the period 1997–2017 on a monthly scale. The red line represents the variability of the spectral power, while the blue line represents the minimum value of significance P0.01 (11.11) and the purple line represents the minimum value of P0.05 (9.48).

Figure 6 shows the spectral analysis of the quarterly series of ITCZ latitude displacement. This result would show a single period of 33 months (almost 3 years) as significant, although it would be below the P0.01 level of significance, but above the P0.05 level.

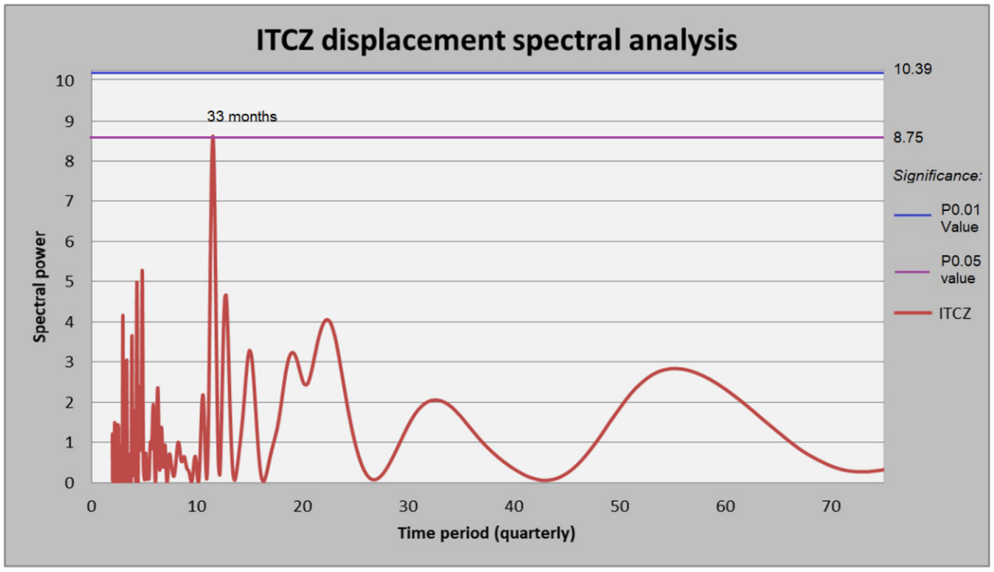

Figure 6. Spectral analysis of the latitudinal shifts of the ITCZ for the period 1979–2005 on a quarterly scale. The red line represents the variability of the spectral power, while the blue line represents the minimum value of significance P0.01 (10.39) and the purple line represents the minimum value of P0.05 (8.75).

Despite the low significance, it was considered as correct, given that the low value of spectral power may be due to a small number of the data series analyzed, that in a greater temporal resolution it could offer a higher significance level.

In the spectral analysis of SALLJ (Figure 7.), up to 6 discernible periodicities were found. Three of them would be below the annual value (12 month): 8.8 months, 4.7 months, and 25 days. Above the annual value, periods of 32 months (2 years and 7 months), 63 months (5 years and 6 months), and 110 months (9 years and 3 months) were found.

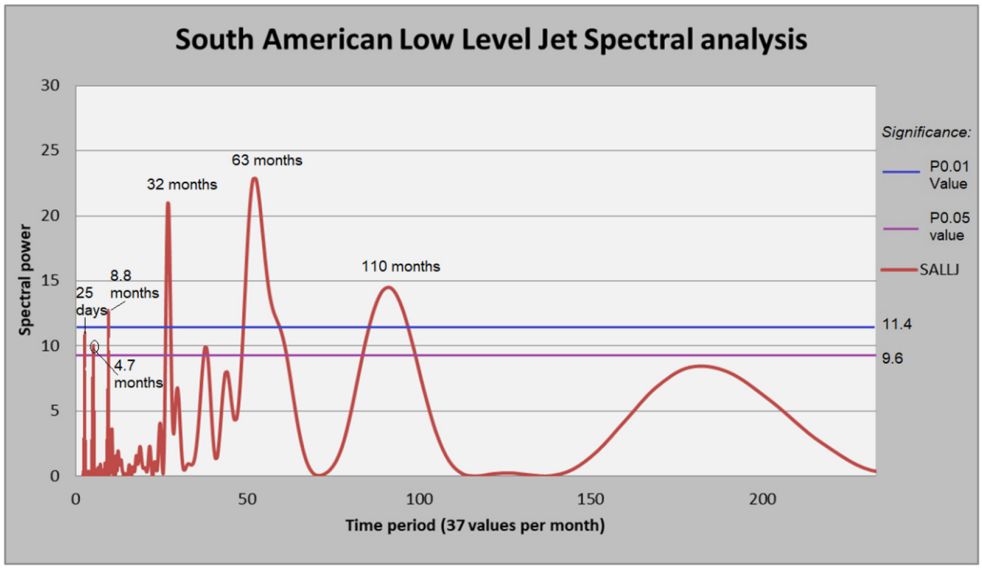

Figure 7. Spectral analysis of the SALLJ intensity for the period 1979–2018 at its own scale in which 37 values correspond to one month. The red line represents the variability of the spectral power, while the blue line represents the minimum value of significance P0.01 (11.4), and the purple line represents the minimum value of P0.05 (9.6).

In the spectral analysis of the MJO (Figure 8), a great variability of high powers and very frequent cycles would be observed. However, among the high frequency of cycles,

a series of periodicities is observed that would "stand out" among the rest, being mainly 7 cycles.

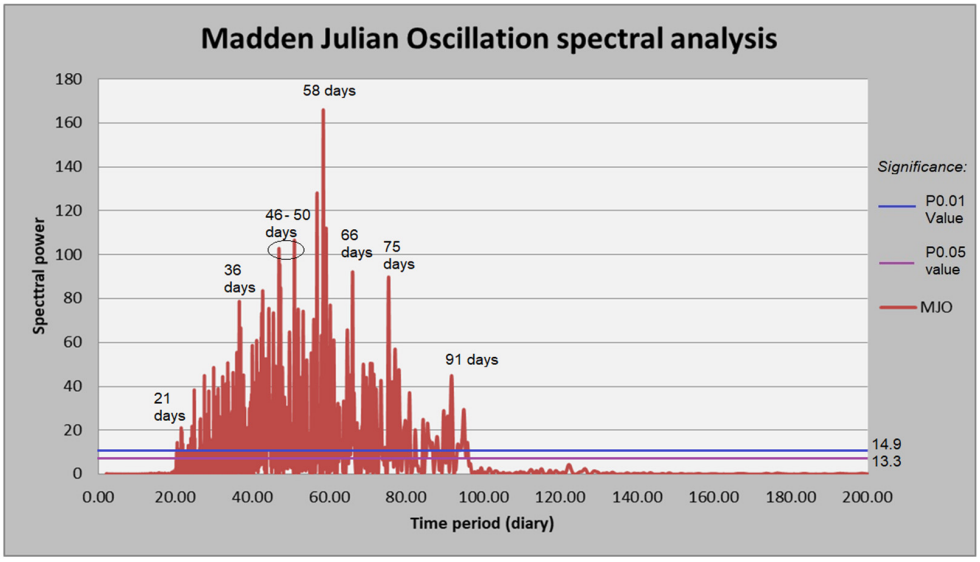

Figure 8. Spectral analysis of the Madden Julian Oscillation for the period 1979–2021 on a daily scale. Red line represents spectral power, P 0.01 (blue line) in 14.9 and P0.05 (purple line) in 13.3.

It is possible to assume that there would be detected cycles every 21 days, 36 days, between 46 and 50 days (1 month and a half), 58 days (1 month and 3 weeks), 66 days (2 months), 75 days (2 and a half months), and 91 days (3 months). Above this 91-day cycle, there would be no more periodicities that exceed the level of significance, indicating that the entire MJO process would have a maximum duration of 91 days.

Spectral analysis of the OLR (Figure 9) showed only one periodicity at 45 days (1 and a half months). Another near 9-month (265 days) cycle is close to the P0.05 significance but still below the level.

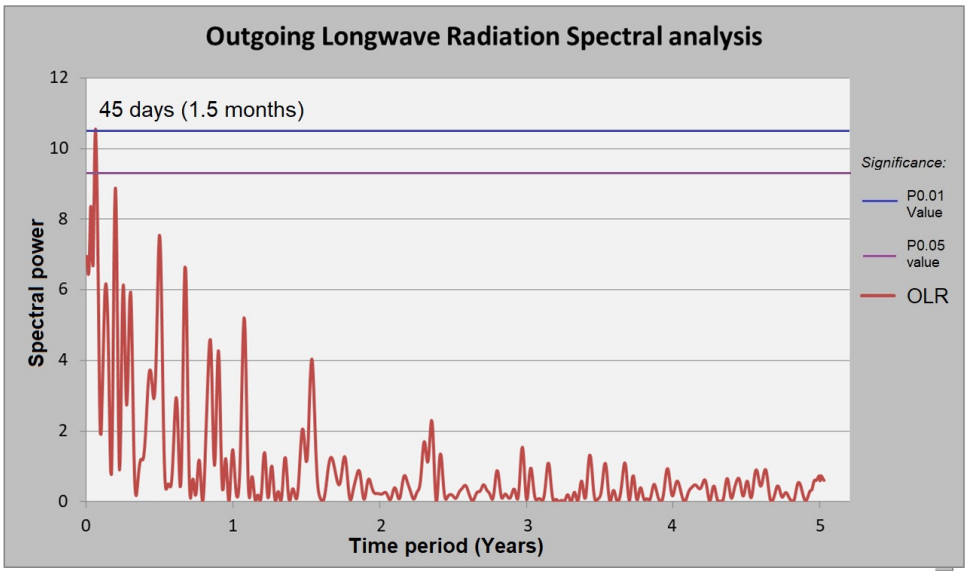

Figure 9. Spectral analysis of the OLR for the period 1999–2014 on a daily scale. P 0.01 (red line) in value 10.7 and P0.05 (purple line) in 9.1.

The data related to the Caribbean Low-Level Jet, the Bolivian High, and the Chocó Low-Level Jet, due to their annual resolution scale, could not be subjected to spectral

analysis, since such a short data series yields errors for powers much lower than the estimated significance. The maximum powers reflected in these analyses were found at spectral values between 4 and 6, with a minimum significance of P0.01 between 11 and 10 and P0.05 between 9.5 and 8.

4.3. Results Synthesis

In the meteorological spectral analysis, up to 3 intraseasonal (27–30 days, 46–52 days, and 90 days), 2 interseasonal (122 days and 182 days), and 1 annual (365 days) periods were found.

The intraseasonal periodicities of 27–30 days would have some coincidence with solar cycles of 27 days [58], while periodicities of 46–52 days and 90 days would match the MJO periodicities here found of 30 days, 45 days (also OLR 45 days), and 91 days. Interseasonal period of 182 days would match the ITCZ periodicity here identified of 182 days. Annual periodicities in the weather records would match the ENSO and SST 1 year periodicities here found.

In longer scales, 6 interannual (1 year and 3 months, 1 year and 6 months, 1 year and 9 months, 3 years, 4.5 years, and 5.6–7 years) and 2 interdecadal (11–12 years and 14–18 years) periodicities were also identified.

The 1 year and 3-month period could match the 1.3 periodicities for Humbold current and SALLJ found in the present work, while the 3-year period could also have connection with the ENSO, SALLJ, and ITCZ displacement, all with a 3-year periodicity. The 4.5 period and period could match the ENSO periodicity here found. The interdecadal period of 11–12 years would be connected to SST, ENSO, and solar variabilities [59], while the 14–18 periods could be little related to PDO variabilities [60].

5. Discussion

Few climatic studies were carried out in the South American region using the spectral analysis technique, being mostly paleoclimatic analysis of sedimentary cores [27] and ice cores [29]. Three different works [30,31,61] with a spectral analysis methodology were found dealing with meteorological records in South America, revealing the lack of this approach for climate analysis.

In Peru, the application of the Lomb periodogram was only applied by the Peruvian Meteorological and Hydrology Service [61] not for the purpose of periodicity analysis, but to determine the probability that the ENSO phenomenon could suffer a change in intensity due to the influence of climate change.

Therefore, the methodology carried out in the present study would be unprecedented in the analyzed territory (Cordillera Blanca). Without the possibility of an adequate comparison of the results (with more similar works), these were compared with the periodicities of the synoptic-scale patterns that could most affect the Cordillera Blanca.

5.1. Intra-Annual Periodicities

The three main periods with a high spectral value and existing in most of the Cordillera Blanca's weather stations for all the variables would be the periods of 122 days (4 months), 182 days (6 months), and 365 days (1 year). The periods of 182 days and 365 days would correspond to cycles present in the data series that would have a biannual and annual character.

The 182-day period found on Cordillera Blanca weather records would have a good correspondence with the patterns of the strengthening/weakening of the Humboldt Current, which, according to the spectral analysis performed in this study, would have a biannual behavior (among others), revealing changes in the current every 6 months.

The 365-day period would be the most powerful and with the greatest presence in all the variables of all the meteorological records. This period would correspond to cycles of similar power and frequency present in almost all the patterns that would act in the Cordillera Blanca. Periodicities of 365 days were observed in the ENSO events, Humboldt

Current enhancement, and Sea Surface Temperature (SST). In this last case, SST could be a primary force by influencing the ENSO and Humboldt Current behaviors [62,63]. While other studies describe an annual periodicity for the ITCZ displacement over Peru [8,64], the present did not find enough significance in this annual periodicity, probably due to a low resolution of the data series for ITCZ.

The 122-day period (4 months), would have a good correspondence with the periodicity found in the strengthening/weakening of the Humboldt Current, as well as in the variability found in this work for the South American Low-Level Jet. This fact would make climate sense, since the period 122-day period is more noticeable in the precipitation variable, being the Humboldt Current the one that could influence the precipitation of the meteorological stations located to the West, while the SALLJ could have a great influence on the precipitation East-facing stations [16,47,65].

The secondary periods detected on a monthly scale would be of 90 days (3 months), 72 days (3 months and 15 days), 46 days (one month and 15 days) and 27 days.

The 72-day period and 90-day period found in Cordillera Blanca would be very close and could be considered as the same cycle. There would be some correspondence with the estimated cyclicity in this study for the MJO (Madden Julian Oscillation), a climate pattern that would have two cycle peaks of 91 and 75 days revealed here. This oscillation occurs in the waters of the Western Pacific and there is still not enough literature linking the MJO with the variability of precipitation or temperature in the South American continent, although some recent research that describes a certain influence on both variables through the greater or lesser propagation of Rossby waves [66,67]. Some influence of the MJO on the variability of precipitation was also described from the activity of the South American Summer Monsoon [68]. In the case of this study, a possible greater influence of the MJO phenomenon on the minimum temperature of Cordillera Blanca would be observed, rather than on the maximum temperature or precipitation, and a notable influence on cloudiness could also be shown.

The secondary period of 46 days observed in this study would correspond to a periodicity of maximum and minimum temperature rather than for precipitation. In this case, a correspondence with the MJO phenomenon would be observed, again, since periodicities of exactly 46 days would be revealed in this climate pattern. However, this would not be the only coincidence, as the Outgoing Longwave Radiation (OLR) variable would also show 45-day cycle as derived from the present work, while some research found that the SST would have warm episodes every 1 or 2 months during the spring season [69,70]. In the case of precipitation in the Amazon basin, periodicities between 1 and 2 months were also found that could be influencing the study area [71], although it would be discarded due to the low number of periodicities found for precipitation. In this work, possibly, all the climate patterns described below would act in a staggered manner, changing in the first instance the temperature of the SST, thus influencing the MJO, which would have an impact on the OLR (clouds) over Cordillera Blanca and which, subsequently, would influence the maximum temperature and minimum from the phenomenon of outgoing energy to the atmosphere and the associated increases or decreases in temperature [72,73].

The secondary periods of 30 and 27 days could be described as the same period as a whole, being a monthly cyclicity present fundamentally in the maximum and minimum temperatures. These cycles would have correspondence to MJO and SALLJ patterns, given the revelation in this study of two 21-day periods for these processes. In turn, several investigations observed solar periodicities of exactly 27 days, which fully coincide with the temperature periodicity revealed here [21,58]. Once again, the solar influence as primary forcing could be induced indirectly through the influence of the MJO and the SALLJ on the temperature variables, and could even directly influence the solar irradiation that would reach the Cordillera Blanca.

5.2. Interannual Periodicities

Other secondary periods would have interannual behavior in the study area, with periodicities found for 479 days (1 year and 3 months), ~550 days (1 year and 6 months), and 635 days (1 year and 9 months).

The meteorological periodicity of 635 days, corresponding to 1 year and 9 months, would not coincide with any of the analyzed climate patterns, although it could be close to the 2-year cyclicity of ENSO events reported by Lu et al. [74]; however, it would not coincide for 3 months, which would be a long period.

The cycle of 479 days corresponding to 1 year and 3 months would correspond to cycles of similar periodicity found in this study for the SALLJ (1 year and 2 months) and the strengthening/weakening of the Humboldt Current (1 year and 4 months). This periodicity would have a greater power for the minimum temperature variable, indicating that the influence of these events would be related to cloud cover and it is probably due to this fact that the coincident climate patterns are two of the most closely related to precipitation. It is possible that the joint influence of both patterns is more intense in the meteorological stations located to the west in the case of the Humboldt Current and for the stations located to the east in the case of the SALLJ, modulating the minimum temperature of both patterns in a similar way, and leaving the common period to be sensitive in the middle of their periodicities (1 year and 3 months) for the entire study area.

The cycle around 550 days (1 year and 6 months) would be revealed mainly for the temperature variable in Cordillera Blanca. In this case, there would not be coincident cycles in the climate patterns analyzed in this study, but the closest period is the strengthening/weakening of the Humboldt Current with 1 year and 4 months. However, the difference of 2 months between the two cycles would lead one to think that there is no connection, or that the link is very soft, between the patterns and the temperature.

The secondary long-term interannual variability periods would be the 1095-day (3 years), 1460-day (4 years), the 1650-day period (4.5 years), and the double period from 1825 to 2555 days (5.6–7 years), the period of 11 years, and the double period of 16 to 17 years.

The period of 1095 days (3 years) would be more visible in the maximum temperature than in the minimum, and no coincidence would be observed for precipitation. This periodicity for Cordillera Blanca records would be coincident with the ENSO climate pattern, the SALLJ, and the ITCZ displacement, which yielded periodicities of 3 years and 3 months in this study. The 3-month lag, with respect to the meteorological periodicity, would be considered normal due to the large amount of data accumulated within the 3-year cycle, unlike previous periodicities that would have a lower data range. The influence of the ITCZ could be higher in this case than the ENSO phenomenon, since the ITCZ climate pattern would be associated with a greater cloud cover of vertical development and cumulus [69], creating a decrease in the maximum temperature in Cordillera Blanca, and therefore allowing the correspondence here hypothesized. It is possible that the frequency of entry of the ITCZ over areas close to the study area is not generating enough precipitation to be detected in a spectral cycle, but it is "pushing" the cloud band southward and influencing the maximum temperature. This observation would coincide with the investigations of Su et al. [75], who observed that the mean high-type cloud cover in the tropics decreased on an interannual scale with the warming of the land surface while OLR and precipitation increased.

The period of 1460 days or 4 years would not have a correspondence with any of the periodicities found in this study, nor with any of the cyclicities consulted in the bibliography.

The periodicity of 1650 days (4.5 years), would be a period with a great imprint in the maximum temperature and slightly in the minimum temperature. This period could have a correspondence with the periodicity observed in this study for the ENSO phenomenon of 4.7–5 years. Some research revealed the existence of a solar cycle of between 5 and 5.5 years [21,76,77]. It would be possible that these solar cycles (especially the 4.7–5-year cycle) were exerting influence as a primary force to be transmitted from the variability of the

ENSO phenomena as a secondary forcing. Even so, the existence of a direct influence of solar irradiation should not be ruled out, since the maximum temperature is a variable highly dependent on irradiation [72,73]. It is likely that the conjunction of both climate patterns (ENSO and solar irradiation) could be influencing the temperature variable, with ENSO events creating a greater or lesser cloud cover and directly influencing solar irradiation from the solar periodicities mentioned.

The double period of 1825 and 2555 days (5.6 to 7 years), found in Cordillera Blanca, would have a greater imprint on the maximum temperature. Even so, some authors [30,74] would indicate the existence of ENSO periods with a cyclicity of 5 to 7 years, as well. However, in the present study, this 7-year periodicity was not found after the spectral analysis of the ONI index data. Certain investigations revealed the existence of a solar cycle of between 5 and 5.5 years [21,76–78], while the existence of a solar periodicity would also determine 7.8 years [21], which would be somewhat far from the double periodicity observed in the meteorological variables of the present study. The greatest probability would be that the conjunction of both climate patterns was influencing the temperature variable, with ENSO events creating a greater or lesser cloud cover and directly influencing solar irradiation from the solar periodicities mentioned.

5.3. Long Term Periodicities

In the long term, the first periodicity calculated would be 11–12 years (4015–4385 days), which would coincide to a greater extent with the minimum temperature compared to the maximum temperature and would have no influence on the periodicity of precipitation. Historically, the 11-year cycle was associated with sunspot variability [22,76–78], which would have a repercussion on the short term temperatures, from the semi-regular increase and decrease of up to 0.15% of the solar intensity, but without much long-term influence [79]. Solar variability, however, could have a broader influence on temperature decreases than on increases [80], a possibility that would explain, according to the results of present work, the greater influence of this period on the minimum temperature than on the maximum temperature. In order to have a greater influence on the maximum temperature than on the minimum, it would be necessary to have a conjunction of the solar periodicity with other climate patterns, such as the OLR and CO_2 [81–83], which would not be reflected in the maximum temperature periodicity.

The correspondences of this 11-year periodicity would not only be with solar variability, but would also coincide with the 11-year ENSO periodicity resulting from the spectral analysis of this study and with the 11-year cyclicity found by Lin et al. [59] in the SST, who also related this solar shift with the SST and ENSO variability. Therefore, the existence of a "cascade" phenomenon would be very likely, whereby the correspondence of the minimum temperatures would be influenced by the triple solar–SST–ENSO phenomenon in a coincidence between all the phenomena.

The last cycle detected in the spectral analysis of the meteorological variables would be the double the cycle of 16 and 17 years, which can be detected in all the variables, both maximum and minimum temperatures, as precipitation. At first, it was thought that this cycle would be an artificial result coinciding with the length of some of the meteorological datasets and the end of the series. This fact was discarded when it was observed that the stations with periodicities of 16–17 years would be those of Huánuco, Oyón, Augusto Weberbahuer, Cachicadán, and Pomabamba, which would be part of the observatories with the longest data series (32 years).

After discarding the above hypothesis, it was observed that the only correspondence with any climate patterns could be with the PDO, which, during warm climatic stages, would have a periodicity of between 12 and 20 years [84]. The influence of the PDO on the temperature of South America was described in different investigations [85], being in turn remotely connected from the ENSO [30,86,87] and the SST [88], climate patterns that could be directly influential to Cordillera Blanca. However, none of these last patterns showed

significant periodicities in the present study that coincided with these PDO cycles, perhaps due to the range of data analyzed.

In a general look, it is possible to affirm that the Humboldt Current, the MJO, the SALLJ, and the OLR would have an intra-annual variability fundamentally, while the solar climate patterns would have inter-annual variability (with the exception of the 27-day cycle) and the decadal PDO. In addition, there would be some patterns that would alternate between inter-annual and intra-annual variability, such as the ITCZ, SST, or ENSO.

5.4. Comparison with Other Regions: Cases of Study

Through spectral analysis, other authors detected periodicities very similar to this study in meteorological records of precipitation and temperature in South America and in other parts of the world. However, the literature is scarce.

Ilyes et al. [31] performed spectral analysis of precipitation series from Ecuador, Kenya, and Hungary. In the area of Ecuador, the Costa, Sierra, and Amazon region revealed periodicities of 365 days and 182 days, which would fully coincide with the main cycles detected in this study.

As secondary cycles in the Amazon regions Ilyes et al. [31] detected periods of 4 months and in the Andean area of 3 months, being in line with the secondary cycles detected in the present work of 90 and 122 days. This 122-day cycle is one of the main cycles and corresponds well with the precipitation in Cordillera Blanca. The 90-day cycle would be observed in general in the Cordillera Blanca, although it would have a greater presence in the stations located to the Northwest of the Cordillera Blanca and a greater power in the Western subregion, being, perhaps, the area closest to Ecuador. The appearance of this cycle in a study area in Ecuador would reinforce the hypothesis that it is the regions closest to the Pacific that would be affected by the MJO climate pattern. A last period of between 2.3 and 2.4 months would appear in the Ecuadorian highlands and Amazon but would not correspond to the cycles detected in this study.

Finally, on the Ecuadorian coast, Ilyes et al. [31] would detect a cycle of 54 months (4.5 years) and another one of 27 months (2 years and 3 months). The cycle of 54 months would have a perfect fit with the cycle of 4.5 years detected in Cordillera Blanca, which would be attributed to the joint influence of the Sun and the ENSO events. The period of 27 months (2 years and 3 months), found in Ecuador, would not correspond to any period detected in Cordillera Blanca.

In turn, the teleconnections that are proposed between Ecuador–Kenya–Hungary [31], could also be related to the Cordillera Blanca region, as periodicities of 1 year are detected for Kenya and Hungary, and of 3 and 4 months for Kenya, indicating that the processes behind these cyclicities could happen on a global scale. Further investigation would be required in this regard.

Recent research on Natuna Island, Indonesia [89], detected some similar cycles for the precipitation variable. Despite the distance between this region and the Cordillera Blanca, there would be some similarities revealed by observing periodicities of 361 days and 177 days that could be close to the periodicities of 365 days and 182 days detected in Cordillera Blanca. While the authors did not assume a clear force behind the 365-day cycle, the 177-day cycle was attributed to possible climate patterns such as the MJO, Borneo vortex, and cold surge. Although the 182-day cycle of the Cordillera Blanca is attributed to the variability of the Humboldt Current without finding close periodicities of the MJO, on Natuna Island, the confluence of the MJO with the other climate patterns could be creating local conditions for a variability of that period, not invalidating the observations made in the present study.

Herho et al. [89], in turn, detected a third period of 1652 days (4.5 years). This period is attributed to the influence of the ENSO events and the Indian Ocean Dipole. This 4.5-year period would have an exact correspondence with the 54-month period found in Ecuador [31] and would be completely consistent with the 4.5-year period found in the present study. The three periods of Indonesia, Ecuador, and Cordillera Blanca would

coincide quite well with the ENSO periodicity of 4.5 years detected in the present work, which could again indicate that the 4.5-year periodicity of the maximum and minimum temperature variables, without being reflected in precipitation, would have a joint influence with some other climate patterns and not only the ENSO. Probably, at least, it could have an indirect and relatively advanced influence (due to the difference of 2.4 months between the ENSO and the meteorological variables of the three regions) in Cordillera Blanca due to less variability, as it is far from the coast. In any case, the periodicity of 4.5 years in the three regions would be jointly attributed to the variability of the ENSO phenomena.

Although some of the main research in the South American climate characterizes the influences of MJO as a dipole influence or a teleconnection [8,90], the present study could find the MJO as one of the more probably matched patterns in the intraseasonal and interseasonal scales, similar to the results found in Herho et al. [89].

5.5. Shortcomings

Some shortcomings have to be taken into consideration. First of all, as data records come from different sources, different time scales were involved in the analysis. Meteorological records are in a daily time scale, as well as sun radiation and the MJO index for climate pattern analysis. Other data records are in a monthly and annual time scales, preventing a correct analysis and not matching with meteorological records, which are on a daily scale. Even so, it was possible to calculate correlations of periodicities for records that originally had different time spans. Annual time scales in the Bolivian High, Caribbean, and Chocó Low-Level Jets prevented the periodogram from calculating periodicities with enough significance. Further research on improving the time span for the climate pattern indexes on an annual scale is recommended in order to find periodicities with enough significance.

Additionally, some of the climate pattern indexes were not renovated since decades ago. The ITCZ displacement index, Bolivian High index, as well as the Caribbean and Chocó Low-Level Jets have values for more than 17 to 12 years before the writing of this work, preventing an actualization of the behavior of these climate patterns. On the other hand, the last decades, in terms of global warming, were the most warmed years in Latin America [91], probably influencing climate pattern behavior. Further research in actualizing these indexes when taking into consideration the periodicity results is needed.

6. Conclusions

Spectral analysis techniques proved to be very useful tools when evaluating the influence of different climate patterns on the regional meteorology and climate of Cordillera Blanca. The common periodicities found, both in the meteorological records and in the records of the different patterns, could be indicative of contemporaneity and joint occurrence. This joint influence allows comparisons to be made for climate variability.

The present study revealed several main periodicities in the climatic records of Cordillera Blanca, counting those of 122, 182, and 365 days. The first cycle (122 days), could come from the influence of the SALLJ and the Humboldt Current, while the second cycle (182 days), would correspond to the periodicity of the displacement towards the south of the ITCZ. The 365-day cycle, the most powerful in all the records, could be due to a joint influence of the ENSO and SST episodes, phenomena that would also be related to each other.

The present work also revealed possible direct and indirect relationships between the MJO–SALLJ systems and the intra- and interseasonal scale periodicities of precipitation and temperature variables. In periodicities with an interannual scale, the main influences could be the ENSO phenomena, influenced by solar activity, as well as the displacement of the ITCZ in the meteorological periodicity of 3 years. Interdecadal cycles could be influenced by PDO and sunspot cycles.

Some issues need to be taken into consideration, especially considering that analyses here made are over different sources with different time scales. Additionally, some of the

climate pattern indexes here analyzed are not renewed from years ago or are not in enough time resolution to show further periodicities.

Further analysis has to be made in other climate patterns, such as the Bolivian High, Caribbean Low-Level Jet, and Chocó Low-Level Jet, revealing the periodicity of these phenomena due to the lack of long enough data series. Knowing the periodicities of these climate patterns and comparing them with the cycles found in the meteorological series could shed light to the possible influence and teleconnections with Cordillera Blanca climate.

Supplementary Materials: The following supporting information can be downloaded at: https://drive.google.com/drive/folders/1pdi-FFGX-VWOJar_8_NOqaPKFJvNsRYP?usp=sharing, (accessed on 4 December 2022) Table S1: Periodicities found for each meteorological variable of each weather station of Cordillera Blanca. Figure S1: Developed code in Rstudio for statistical imputation of missing values.

Author Contributions: Conceptualization, A.F.-S. and J.Ú.; methodology, A.F.-S.; software, A.F.-S.; validation, J.Ú., L.M.T. and J.A.Á.-A.; formal analysis, A.F.-S. and N.N.-F.; investigation, A.F.-S.; resources, J.I.; data curation, A.F.-S., J.I. and N.N.-F.; writing—original draft preparation, A.F.-S.; writing—review and editing, All authors.; funding acquisition, J.Ú. All authors have read and agreed to the published version of the manuscript.

Funding: This research was funded by PERMAFROST ENSO O81-2021-FONDECYT (75941) project through Peru's Ministry of Education.

Institutional Review Board Statement: Not applicable.

Informed Consent Statement: Not applicable.

Data Availability Statement: Available data can be found at SENAMHI (https://www.senamhi.gob.pe/servicios/?p=descarga-datos-meteorologicos), accessed on 21 March 2020) and NOAA (https://www.ncdc.noaa.gov/cdo-web/datasets) websites.

Acknowledgments: We thank the anonymous reviewers and the Atmosphere team for the comments and improvement done on this research paper. We thank SENAMHI meteorological service for the data provision. We also appreciate the Cryoperú project and KFA association for the support provided.

Conflicts of Interest: The authors declare no conflict of interest. The funders had no role in the design of the study; in the collection, analyses, or interpretation of data; in the writing of the manu-script; or in the decision to publish the results.

References

1. Beer, J.; Mende, W.; Stellmacher, R. The Role of the Sun in Climate Forcing. *Quat. Sci. Rev.* **2000**, *19*, 403–415. [CrossRef]
2. Xiong, Z.; Li, T.; Chang, F.; Algeo, T.J.; Clift, P.D.; Bretschneider, L.; Lu, Z.; Zhu, X.; Frank, M.; Sauer, P.E.; et al. Rapid Precipitation Changes in the Tropical West Pacific Linked to North Atlantic Climate Forcing during the Last Deglaciation. *Quat. Sci. Rev.* **2018**, *197*, 288–306. [CrossRef]
3. Tilmes, S.; Hodzic, A.; Emmons, L.K.; Mills, M.J.; Gettelman, A.; Kinnison, D.E.; Park, M.; Lamarque, J.-F.; Vitt, F.; Shrivastava, M.; et al. Climate Forcing and Trends of Organic Aerosols in the Community Earth System Model (CESM2). *J. Adv. Model. Earth Syst.* **2019**, *11*, 4323–4351. [CrossRef]
4. Richardson, T.B.; Forster, P.M.; Smith, C.J.; Maycock, A.C.; Wood, T.; Andrews, T.; Boucher, O.; Faluvegi, G.; Fläschner, D.; Hodnebrog, Ø.; et al. Efficacy of Climate Forcings in PDRMIP Models. *J. Geophys. Res. Atmos.* **2019**, *124*, 12824–12844. [CrossRef]
5. O'Neel, S.; McNeil, C.; Sass, L.C.; Florentine, C.; Baker, E.H.; Peitzsch, E.; McGrath, D.; Fountain, A.G.; Fagre, D. Reanalysis of the US Geological Survey Benchmark Glaciers: Long-Term Insight into Climate Forcing of Glacier Mass Balance. *J. Glaciol.* **2019**, *65*, 850–866. [CrossRef]
6. Scott, R.C.; Nicolas, J.P.; Bromwich, D.H.; Norris, J.R.; Lubin, D. Meteorological Drivers and Large-Scale Climate Forcing of West Antarctic Surface Melt. *J. Clim.* **2019**, *32*, 665–684. [CrossRef]
7. Takano, Y.; Ito, T.; Deutsch, C. Projected Centennial Oxygen Trends and Their Attribution to Distinct Ocean Climate Forcings. *Glob. Biogeochem. Cycles* **2018**, *32*, 1329–1349. [CrossRef]
8. Garreaud, R.D. The Andes Climate and Weather. *Adv. Geosci.* **2009**, *22*, 3–11. [CrossRef]
9. Veblen, T.; Young, K.; Orme, A. *The Physical Geography of South America*, 1st ed.; Oxford University Press: New York, NY, USA, 2007; ISBN 978-0-19-531341-3.

10. Samanta, D.; Karnauskas, K.B.; Goodkin, N.F. Tropical Pacific SST and ITCZ Biases in Climate Models: Double Trouble for Future Rainfall Projections? *Geophys. Res. Lett.* **2019**, *46*, 2242–2252. [CrossRef]
11. Williams, I.N.; Patricola, C.M. Diversity of ENSO Events Unified by Convective Threshold Sea Surface Temperature: A Nonlinear ENSO Index. *Geophys. Res. Lett.* **2018**, *45*, 9236–9244. [CrossRef]
12. IPCC; Arias, P.A.; Allan, R.P.; Armour, K.; Barimalala, R.; Canadell, J.G.; Cassou, C.; Cherchi, A.; Collins, W.; Corti, S.; et al. *Climate Change 2021: The Physical Science Basis. Contribution of Working Group I to the Sixth Assessment Report of the Intergovernmental Panel on Climate Change*; Intergovernmental Panel on Climate Change: Cambridge, UK; New York, NY, USA, 2021; p. 2409.
13. Iturbide, M.; Gutiérrez, J.M.; Alves, L.M.; Bedia, J.; Cerezo-Mota, R.; Cimadevilla, E.; Cofiño, A.S.; Di Luca, A.; Faria, S.H.; Gorodetskaya, I.V.; et al. An Update of IPCC Climate Reference Regions for Subcontinental Analysis of Climate Model Data: Definition and Aggregated Datasets. *Earth Syst. Sci. Data* **2020**, *12*, 2959–2970. [CrossRef]
14. IPCC; Stocker, T.F.; Qin, D.; Plattner, G.-K.; Tignor, M.; Allen, S.K.; Boschung, J.; Nauels, A.; Xia, Y.; Bex, V.; et al. *Climate Change 2013: The Physical Science Basis. Contribution of Working Group I to the Fifth Assessment Report of the Intergovernmental Panel on Climate Change*; Intergovernmental Panel on Climate Change: Cambridge, UK; New York, NY, USA, 2013; p. 1585.
15. Sulca, J.; Takahashi, K.; Espinoza, J.-C.; Vuille, M.; Lavado-Casimiro, W. Impacts of Different ENSO Flavors and Tropical Pacific Convection Variability (ITCZ, SPCZ) on Austral Summer Rainfall in South America, with a Focus on Peru. *Int. J. Climatol.* **2018**, *38*, 420–435. [CrossRef]
16. Jones, C.; Carvalho, L.M.V. The Influence of the Atlantic Multidecadal Oscillation on the Eastern Andes Low-Level Jet and Precipitation in South America. *Npj Clim. Atmospheric. Sci.* **2018**, *1*, 40. [CrossRef]
17. Cai, W.; McPhaden, M.J.; Grimm, A.M.; Rodrigues, R.R.; Taschetto, A.S.; Garreaud, R.D.; Dewitte, B.; Poveda, G.; Ham, Y.-G.; Santoso, A.; et al. Climate Impacts of the El Niño–Southern Oscillation on South America. *Nat. Rev. Earth Environ.* **2020**, *1*, 215–231. [CrossRef]
18. Bauer, E.; Claussen, M.; Brovkin, V.; Huenerbein, A. Assessing Climate Forcings of the Earth System for the Past Millennium: Climate Simulations for Past Millennium. *Geophys. Res. Lett.* **2003**, *30*, 1–9. [CrossRef]
19. Lomb, N.R. Least-Squares Frequency Analysis of Unequally Spaced Data. *Astrophys. Space Sci.* **1976**, *39*, 447–462. [CrossRef]
20. Zhao, X.; Soon, W.; Velasco Herrera, V.M. Evidence for Solar Modulation on the Millennial-Scale Climate Change of Earth. *Universe* **2020**, *6*, 153. [CrossRef]
21. Zhu, F.R.; Jia, H.Y. Lomb–Scargle Periodogram Analysis of the Periods around 5.5 Year and 11 Year in the International Sunspot Numbers. *Astrophys. Space Sci.* **2018**, *363*, 138. [CrossRef]
22. Pezzopane, M.; Pignalberi, A.; Pietrella, M. On the Influence of Solar Activity on the Mid-Latitude Sporadic E Layer. *J. Space Weather Space Clim.* **2015**, *5*, A31. [CrossRef]
23. Akdi, Y.; Gölveren, E.; Ünlü, K.D.; Yücel, M.E. Modeling and Forecasting of Monthly PM2.5 Emission of Paris by Periodogram-Based Time Series Methodology. *Environ. Monit. Assess.* **2021**, *193*, 622. [CrossRef] [PubMed]
24. Aldegunde, J.A.Á.; Fernández-Sánchez, A.; Saba, M.; Bolaños, E.Q.; Caraballo, L.R. Spatiotemporal Analysis of PM2.5 Concentrations on the Incidence of Childhood Asthma in Developing Countries: Case Study of Cartagena de Indias, Colombia. *Atmosphere* **2022**, *13*, 1383. [CrossRef]
25. Froyland, G.; Giannakis, D.; Lintner, B.R.; Pike, M.; Slawinska, J. Spectral Analysis of Climate Dynamics with Operator-Theoretic Approaches. *Nat. Commun.* **2021**, *12*, 6570. [CrossRef] [PubMed]
26. Akdi, Y.; Ünlü, K.D. Periodicity in Precipitation and Temperature for Monthly Data of Turkey. *Theor. Appl. Climatol.* **2021**, *143*, 957–968. [CrossRef]
27. Lamy, F.; Hebbeln, D.; Röhl, U.; Wefer, G. Holocene Rainfall Variability in Southern Chile: A Marine Record of Latitudinal Shifts of the Southern Westerlies. *Earth Planet. Sci. Lett.* **2001**, *185*, 369–382. [CrossRef]
28. Warner, R.M.; Neumann, P.G. SPAN: An Interactive BASIC Program for Spectral Analysis of Time-Series Data. *Behav. Res. Methods Instrum.* **1980**, *12*, 389–390. [CrossRef]
29. Fernández-Sánchez, A.; Martín-Chivelet, J. Revisión de la estratigrafía del δ 18 O en sondeos de hielo de glaciares de los Andes Centrales: Implicaciones para la variabilidad climática del Holoceno. In Proceedings of the Geotemas, Huelva, Spain, 12–14 September 2016; Volume 16, pp. 565–568.
30. Canedo-Rosso, C.; Uvo, C.B.; Berndtsson, R. Precipitation Variability and Its Relation to Climate Anomalies in the Bolivian Altiplano. *Int. J. Climatol.* **2018**, *39*, 2096–2107. [CrossRef]
31. Ilyes, C.; Wendo, V.A.J.A.; Flores Carpio, Y.; Szucs, P. Differences and Similarities between Precipitation Patterns of Different Climates. *Acta Geod. Geophys.* **2021**, *56*, 781–800. [CrossRef]
32. Eguiguren-Velepucha, P.A.; Chamba, J.A.M.; Aguirre Mendoza, N.A.; Ojeda-Luna, T.L.; Samaniego-Rojas, N.S.; Furniss, M.J.; Howe, C.; Aguirre Mendoza, Z.H. Tropical Ecosystems Vulnerability to Climate Change in Southern Ecuador. *Trop. Conserv. Sci.* **2016**, *9*, 194008291666800. [CrossRef]
33. Deb, J.; Phinn, S.; Butt, N.; McAlpine, C. Climate Change Impacts on Tropical Forests. *For. Res. Inst. Malays.* **2018**, *30*, 182–194.
34. INAIGEM. *Informe de la Situación de los Glaciares y Ecosistemas de Montaña en el Perú*; Instituto Nacional de Investigación en Glaciares y Ecosistemas de Montaña del Perú: Huaraz, Peru, 2017; p. 124.
35. Ames Marquez, A.; Francou, B. Cordillera Blanca: Glaciares En La Historia. *Bull. Inst. Fr. Etudes Andin.* **1995**, *24*, 37–64. [CrossRef]
36. SENAMHI. *Climas del Perú: Mapa de Clasificación Climática Nacional*; Servicio Nacional de Meteorología e HIdrología del Perú: Lima, Peru, 2020; p. 70.

37. Kaser, G.; Osmaston, H. *Tropical Glaciers*, 1st ed.; International Hydrology Series; Cambridge University Press: Cambridge, UK, 2002; ISBN 0-521-63333-8.
38. Autoridad Nacional del Agua; Unidad de Glaciología y Recursos Hídricos. *Inventario nacional de glaciares y lagunas: Lagunas*; Autoridad Nacional del Agua: Huaraz, Peru, 2014; p. 21.
39. Instituto Nacional de Estadística e Informática. INEI Censo de Población y Vivienda: Ancash. 2018. Available online: www.inei.gob.pe (accessed on 3 December 2022).
40. Cano, A.; Mendoza, W.; Castillo, S.; Morales, M.; La Torre, M.I.; Aponte, H.; Delgado, A.; Valencia, N.; Vega, N. Flora y vegetación de suelos crioturbados y hábitats asociados en la Cordillera Blanca, Ancash, Perú. *Rev. Peru. Biol.* **2011**, *17*, 095–0103. [CrossRef]
41. NOAA Oceanic El NIño Index. Available online: https://www.cpc.ncep.noaa.gov/data/indices/oni.ascii.txt (accessed on 20 February 2022).
42. Huang, X.; Zhou, T.; Dai, A.; Li, H.; Li, C.; Chen, X.; Lu, J.; Von Storch, J.-S.; Wu, B. South Asian Summer Monsoon Projections Constrained by the Interdecadal Pacific Oscillation. *Sci. Adv.* **2020**, *6*, eaay6546. [CrossRef]
43. Marrari, M.; Piola, A.R.; Valla, D. Variability and 20-Year Trends in Satellite-Derived Surface Chlorophyll Concentrations in Large Marine Ecosystems around South and Western Central America. *Front. Mar. Sci.* **2017**, *4*, 372. [CrossRef]
44. Hidalgo, H.G.; Durán-quesada, A.M.; Amador, J.A.; Alfaro, E.J. The Caribbean Low-level Jet, the Inter-tropical Convergence Zone and Precipitation Patterns in the Intra-americas Sea: A Proposed Dynamical Mechanism. *Geogr. Ann. Ser. Phys. Geogr.* **2015**, *97*, 41–59. [CrossRef]
45. Lee, H.-T. *NOAA CDR Program NOAA Climate Data Record (CDR) of Daily Outgoing Longwave Radiation (OLR), Version 1.2*. 2014.
46. Reason, C.J.C. The Bolivian, Botswana, and Bilybara Highs and Southern Hemisphere Drought/Floods. *Geophys. Res. Lett.* **2016**, *43*, 1280–1286. [CrossRef]
47. Jones, C. Recent Changes in the South America Low-Level Jet. *Npj Clim. Atmos. Sci.* **2019**, *2*, 20. [CrossRef]
48. Sierra, J.P.; Arias, P.A.; Durán-Quesada, A.M.; Tapias, K.A.; Vieira, S.C.; Martínez, J.A. The Choco Low-level Jet: Past, Present and Future. *Clim. Dyn.* **2021**, *56*, 2667–2692. [CrossRef]
49. Xue, Y.; Higgins, W.; Kousky, V. Influences of the Madden Julian Oscillations on Temperature and Precipitation in North America during ENSO-Neutral and Weak ENSO Winters. In *Proc. Workshop on Prospects for Improved Forecasts of Weather and Short-Term Climate Variability on Subseasonal (2 Week to 2 Month) Time Scales*; NASA/Goddard Space Flight Center: Greenbelt, MD, USA, 2002; p. 4.
50. Polanco Martínez, J. *Aplicación de Técnicas Estadísticas en el Estudio de Fenómenos Ambientales y Ecosistémicos*; Universidad del País Vasco, Facultad de Ciencia y Tecnología, Departamento de Física Aplicada II. Leioa: Vizcaya, Spain, 2011.
51. Paulhus, J.L.H.; Kohler, M.A. Interpolation of Missing Precipitation Records. *Mon. Weather Rev.* **1952**, *80*, 129–133. [CrossRef]
52. Enders, C.K. Methodology in the social sciences. In *Applied Missing Data Analysis*, 1st ed.; Guilford Press: New York, NY, USA, 2010; ISBN 978-1-60623-639-0.
53. RStudio Team. *Integrated Development for R, PBC*; RStudio Team: Boston, MA, USA, 2020; Available online: http://www.rstudio.com/ (accessed on 1 July 2021).
54. James, G.; Written, D.; Hastie, T.; Tibshirani, R. *An Introduction to Statistical Learning with Applications in R*, 2nd ed.; Springer Science and Business Media: New York, NY, USA, 2021; Volume 6, ISBN 978-1-07-161417-4.
55. Warner, R.M. *Spectral Analysis of Time-Series Data (Methodology in the Social Sciences)*, 1st ed.; Guilford Press: New York, USA, 1999; ISBN 978-1-57230-338-6.
56. Li, L.; Li, K.; Liu, C.; Liu, C. Comparison of Detrending Methods in Spectral Analysis of Heart Rate Variability. *Res. J. Appl. Sci. Eng. Technol.* **2011**, *3*, 1014–1021.
57. Hammer, O.; Harper, D.A.T.; Ryan, P.D. PAST: Paleontological Statistics Software Package for Education and Data Analysis. *Palaeontol. Electron.* **2001**, *4*, 9.
58. Miyahara, H.; Aono, Y.; Kataoka, R. Searching for the 27-Day Solar Rotational Cycle in Lightning Events Recorded in Old Diaries in Kyoto from the 17th to 18th Century. *Ann. Geophys.* **2017**, *35*, 1195–1200. [CrossRef]
59. Lin, Y.; Yu, J.; Wu, C.; Zheng, F. The Footprint of the 11-Year Solar Cycle in Northeastern Pacific SSTs and Its Influence on the Central Pacific El Niño. *Geophys. Res. Lett.* **2021**, *48*, e2020GL091369. [CrossRef]
60. Maruyama, F.; Kai, K.; Morimoto, H. Wavelet-Based Multifractal Analysis on a Time Series of Solar Activity and PDO Climate Index. *Adv. Space Res.* **2017**, *60*, 1363–1372. [CrossRef]
61. SENAMHI. *Escenarios del Cambio Climático en el Perú al 2050: Cuenca del Río Piura*; Servicio Nacional de Meteorología e HIdrología del Perú: Lima, Peru, 2005; p. 197.
62. Gutiérrez, D.; Akester, M.; Naranjo, L. Productivity and Sustainable Management of the Humboldt Current Large Marine Ecosystem under Climate Change. *Environ. Dev.* **2016**, *17*, 126–144. [CrossRef]
63. Xie, X.; Zhou, S.; Zhang, J.; Huang, P. The Role of Background SST Changes in the ENSO-Driven Rainfall Variability Revealed from the Atmospheric Model Experiments in CMIP5/6. *Atmos. Res.* **2021**, *261*, 105732. [CrossRef]
64. Mamalakis, A.; Randerson, J.T.; Yu, J.-Y.; Pritchard, M.S.; Magnusdottir, G.; Smyth, P.; Levine, P.A.; Yu, S.; Foufoula-Georgiou, E. Zonally Contrasting Shifts of the Tropical Rain Belt in Response to Climate Change. *Nat. Clim. Change* **2021**, *11*, 143–151. [CrossRef] [PubMed]
65. Montini, T.L.; Jones, C.; Carvalho, L.M.V. The South American Low-Level Jet: A New Climatology, Variability, and Changes. *J. Geophys. Res. Atmos.* **2019**, *124*, 1200–1218. [CrossRef]

66. Alvarez, M.; Vera, C.S.; Kiladis, G.; Liebmann, B. Influence of the Madden Julian Oscillation on Precipitation and Surface Air Temperature in South America. *Clim. Dyn.* **2015**, *46*, 245–262. [CrossRef]
67. Alvarez, M.; Vera, C.; Kiladis, G. MJO Modulating the Activity of the Leading Mode of Intraseasonal Variability in South America. *Atmosphere* **2017**, *8*, 232. [CrossRef]
68. Grimm, A.M. Interannual Climate Variability in South America: Impacts on Seasonal Precipitation, Extreme Events, and Possible Effects of Climate Change. *Stoch. Environ. Res. Risk Assess.* **2011**, *25*, 537–554. [CrossRef]
69. Cess, R.D.; Zhang, M.; Wielicki, B.A.; Young, D.F.; Zhou, X.-L.; Nikitenko, Y. The Influence of the 1998 El Niño upon Cloud-Radiative Forcing over the Pacific Warm Pool. *J. Clim.* **2001**, *14*, 2129–2137. [CrossRef]
70. Song, Z.; Liu, H.; Chen, X. Eastern Equatorial Pacific SST Seasonal Cycle in Global Climate Models: From CMIP5 to CMIP6. *Acta Oceanol. Sin.* **2020**, *39*, 50–60. [CrossRef]
71. Carrillo, C.M. The Rainfall over Tropical South America Generated by Multiple Scale Processes. Master's Thesis, Iowa State University, Digital Repository, Ames, IA, USA, 2010; p. 2807786.
72. Huang, Y.; Ramaswamy, V.; Soden, B. An Investigation of the Sensitivity of the Clear-Sky Outgoing Longwave Radiation to Atmospheric Temperature and Water Vapor. *J. Geophys. Res. Atmos.* **2007**, *112*, 13. [CrossRef]
73. Kluft, L.; Dacie, S.; Brath, M.; Buehler, S.; Stevens, B. Temperature-Dependence of the Clear-Sky Feedback in Radiative-Convective Equilibrium. *Geophys. Res. Lett.* **2021**, *48*, 10. [CrossRef]
74. Lu, B.; Jin, F.-F.; Ren, H.-L. A Coupled Dynamic Index for ENSO Periodicity. *J. Clim.* **2018**, *31*, 16. [CrossRef]
75. Su, H.; Jiang, J.; Neelin, D.; Shen, J.; Zhai, C.; Yue, Q.; Wang, Z.; Huang, L.; Choi, Y.-S.; Stephens, G.; et al. Tightening of Tropical Ascent and High Clouds Key to Precipitation Change in a Warmer Climate. *Nat. Commun.* **2017**, *8*, 9. [CrossRef]
76. Hathaway, D.H. The Solar Cycle. *Living Rev. Sol. Phys.* **2015**, *12*, 4. [CrossRef]
77. Chowdhury, P.; Choudhary, D.P.; Gosain, S.; Moon, Y.-J. Short-Term Periodicities in Interplanetary, Geomagnetic and Solar Phenomena during Solar Cycle 24. *Astrophys. Space Sci.* **2015**, *356*, 7–18. [CrossRef]
78. Chowdhury, P.; Dwivedi, B.N. Periodicities of Sunspot Number and Coronal Index Time Series During Solar Cycle 23. *Sol. Phys.* **2011**, *270*, 365–383. [CrossRef]
79. Feliks, Y.; Small, J.; Ghil, M. Global Oscillatory Modes in High-end Climate Modeling and Reanalyses. *Clim. Dyn.* **2021**, *57*, 3385–3411. [CrossRef]
80. Martín-Chivelet, J. *Cambios Climáticos: Una Aproximación al Sistema Tierra.*; Fondo de Cultura Económica: Madrid, Spain, 1999; Volume 1, ISBN 84-7954-542-9.
81. Griggs, J.A.; Harries, J.E. *Comparison of Spectrally Resolved Outgoing Longwave Data between 1970 and Present*; Strojnik, M., Ed.; University of Bristol: Denver, CO, USA, 2004; p. 164.
82. Koll, D.D.B.; Cronin, T.W. Earth's Outgoing Longwave Radiation Linear Due to H_2O Greenhouse Effect. *Proc. Natl. Acad. Sci. USA* **2018**, *115*, 10293–10298. [CrossRef]
83. Manabe, S. Role of Greenhouse Gas in Climate Change. *Tellus Dyn. Meteorol. Oceanogr.* **2019**, *71*, 1620078. [CrossRef]
84. Zhang, L.; Delworth, T.L. Simulated Response of the Pacific Decadal Oscillation to Climate Change. *J. Clim.* **2016**, *29*, 5999–6018. [CrossRef]
85. Kayano, M.T.; Andreoli, R.V. Relations of South American Summer Rainfall Interannual Variations with the Pacific Decadal Oscillation. *Int. J. Climatol.* **2007**, *27*, 531–540. [CrossRef]
86. Gamelin, B.L.; Carvalho, L.M.V.; Jones, C. Evaluating the Influence of Deep Convection on Tropopause Thermodynamics and Lower Stratospheric Water Vapor: A RELAMPAGO Case Study Using the WRF Model. *Atmos. Res.* **2022**, *267*, 105986. [CrossRef]
87. Reboita, M.S.; Ambrizzi, T.; Crespo, N.M.; Dutra, L.M.M.; Ferreira, G.W.d.S.; Rehbein, A.; Drumond, A.; da Rocha, R.P.; Souza, C.A. de Impacts of Teleconnection Patterns on South America Climate. *Ann. N. Y. Acad. Sci.* **2021**, *1504*, 116–153. [CrossRef]
88. Wang, Y.-L.; Hsu, Y.-C.; Lee, C.-P.; Wu, C.-R. Coupling Influences of ENSO and PDO on the Inter-Decadal SST Variability of the ACC around the Western South Atlantic. *Sustainability* **2019**, *11*, 4853. [CrossRef]
89. Herho, S.; Fajary, F.; Irawan, D. On the Statistical Learning Analysis of Rain Gauge Data over the Natuna Islands. *Indones. J. Stat. Its Appl.* **2022**, *6*, 347–357. [CrossRef]
90. Nogués-Paegle, J.; Mechoso, C.R.; Fu, R.; Berbery, E.H.; Chao, W.C.; Chen, T.-C.; Cook, K.; Diaz, A.F.; Enfield, D.; Ferreira, R.; et al. Progress in Panamerican Clivar Research: Understanding the South American Monsoon System. *Meteorologica* **2002**, *27*, 3–32.
91. WMO. *State of the Climate in Latin America and the Caribbean 2021*; World Meteorological Organization: Geneva, Switzerland, 2021; p. 44.